

arXiv:2601.09574v1 [physics.acc-ph] 14 Jan 2026

Square matrix-based six-dimensional convergence map for nonlinear beam dynamics analysis

Jinyu Wan* and Yue Hao†

Facility for Rare Isotope Beams, Michigan State University, East Lansing, 48824, USA

(Dated: January 15, 2026)

Abstract

The square matrix-based convergence map (CM) method has proven effective in characterizing nonlinear dynamics in several 4-D dynamical systems. However, when time-dependent perturbations, such as crabbing kicks in colliders, are present, a comprehensive 6-D analysis becomes essential to accurately capture the coupling between transverse and longitudinal motions. In this work, we extend the CM method to the full 6-D phase space by employing an eigen-decomposition-based formulation of the square matrix combined with iterative procedures. The proposed 6-D CM approach is first validated using a simplified crabbing map. We demonstrate that the 6-D CM preserves computational efficiency by using only one-turn map, while successfully resolving high-order resonance structures that remain unresolved by conventional frequency map analysis (FMA). This method is subsequently applied to the dynamic aperture (DA) study of the future Electron-Ion Collider (EIC). The results obtained from the CM analysis exhibit close agreement with those derived from FMA, demonstrating its potential as a powerful tool for nonlinear beam dynamics analysis and DA evaluation, as well as for broader applications in other nonlinear dynamical systems.

I. INTRODUCTION

Understanding long-term stability in nonlinear dynamical systems remains a critical challenge, particularly in the context of particle accelerators. Currently, particle tracking remains the most reliable approach for studying long-term particle behavior, which is often computationally intensive. Over the past decades, researchers have developed faster techniques for predicting long-term stability, such as canonical perturbation theory, Lie operator methods, power series expansions, and normal form [1–9]. However, these methods often suffer from limited accuracy due to insufficient expansion orders, complications from resonance crossings, or inaccuracies at large amplitudes. For particles undergoing quasi-periodical motion, frequency map analysis(FMA) based on Numerical Analysis of Fundamental Frequencies (NAFF) [10] has been applied on a grid of initial conditions to retrieve the shifts of the dominant frequency, as an indicator for identifying the stable region, resonances and chaotic zones. More recently, data-driven indicators have also been investigated, including round-

* wan@frib.msu.edu

† haoy@frib.msu.edu

off error in forward-reversal integration [11] and machine learning-based stability evaluation [12], offering an alternative approach to the study of beam dynamics.

In recent years, notable work has been made in the application of the square-matrix method [13] for the efficient analysis of periodic nonlinear dynamical systems, particularly in the identification of high-order resonances. Based on this foundation, the convergence map (CM) method was developed [14]. The CM method employs an iterative transformation that converts nonlinear trajectories into a nearly rigid rotational motion, with the residual convergence error serving as an indicator of stability. This framework has been successfully validated in several 4-D dynamical systems, including the 4-D Henon map [15] and the transverse dynamics of the NSLS-II storage ring [16, 17]. Compared with conventional particle tracking and FMA techniques, the CM method offers much faster computational efficiency as it only requires one-turn transfer map in the calculation.

In modern ring colliders, synchro-betatron coupling between transverse and longitudinal dynamics arises from various effects such as accelerating cavities located at dispersive location, beam-beam interactions and other transverse fields with arriving time dependence. In recent collider designs, the hadron beam is designed to collide with another hadron beam or electron beam, such as the LHC high luminosity upgrade and the Electron-Ion Collider (EIC) [18] project. Crab cavities, which provide a time-dependent dipole field, are used to compensate for the loss of geometric luminosity due to the crossing angle. Previous studies show that the high harmonic magnetic moment in the crab cavity will affect the dynamic aperture [19], and might generate additional resonance lines affecting long-term stability of the beam [20]. Using a reduced 4-D analysis can be insufficient to capture such effects.

In this work, we extend the CM from 4-D to the full 6-D phase space to study these synchro-betatron coupling effects. The proposed 6-D CM formulation is based on eigen-decomposition of the one-turn transfer map, enabling more accurate reconstruction of an upper triangular square matrix compared with the Courant-Snyder form in the original 4-D CM method. By combining this formulation with iterative convergence analysis, we reconstruct approximate action-angle variables that capture the invariant tori in the coupled 6-D space. This extension allows the CM to identify subtle high-order resonances and nonlinear couplings that cannot be resolved through conventional FMA. The approach is first validated using a simplified crabbing map containing time-dependent multipole components and is subsequently applied to the hadron storage ring of the EIC to evaluate its dynamic

aperture and the influence of nonlinear crab cavity fields.

The content is organized as follows. A detailed description of the 6-D CM method will be given in Section II. The method will then be implemented on a simplified 6-D nonlinear map, abstracted from crab cavity kicks, in Section III. In Section IV, this method is also applied to the hadron storage ring of the EIC to study the impact of multipole components in crab cavities and evaluate its dynamic aperture.

II. METHOD

A. Approximated action-angle variables using square matrix

For periodic dynamical systems, such as synchrotron accelerators, the one-turn map can be expressed as a set of polynomial equations and rewritten as a square matrix. For a n -D dynamical system described by the canonical variable \mathbf{x} and its momentum \mathbf{p} , if we use the complex Courant-Snyder variable $z = \frac{x}{\sqrt{\beta}} - \frac{i}{\sqrt{\beta}}(\alpha x + p)$ and its conjugate z^* to replace x and p , $\{z, z^*, z^2, zz^*, z^{*2}, z^3, \dots\}$ will form a new column Z where the one-turn map can be described by a square matrix M ,

$$Z = MZ_0. \quad (1)$$

All square matrices can be transformed into Jordan form with a transformation matrix U , an eigenvalue μ , and a Jordan matrix τ [21]

$$UM = e^{i\mu I + \tau}U, \quad (2)$$

where I is the identity matrix and the Jordan matrix has the form

$$\tau = \begin{bmatrix} 0 & 1 & 0 & \dots & 0 \\ 0 & 0 & 1 & \dots & 0 \\ 0 & 0 & \dots & \dots & 0 \\ 0 & 0 & 0 & \dots & 1 \\ 0 & 0 & 0 & \dots & 0 \end{bmatrix}. \quad (3)$$

Then Eq. 1 gives

$$UZ = UMZ_0 = e^{i\mu I + \tau}UZ_0. \quad (4)$$

A transformation is defined as

$$W \equiv UZ, \quad (5)$$

where W represents the projection of Z onto the invariant subspace spanned by the left eigenvectors u_j given by the rows of the matrix U . Therefore, each row of W is represented as $w_j = u_j Z$, which is a polynomial of $\{z, z*, \dots\}$.

The new vector after n now becomes

$$W = e^{n(i\mu I + \tau)} W_0. \quad (6)$$

KAM theory [22] states that an invariant torus is stable under small perturbations. The invariant torus will deform and survive to form a quasiperiodic motion under sufficiently small amplitude. The equation is nearly linear, and the absolute value of each row $|w_j| = |u_j Z|$ is approximately invariant with a phase advance $\mu + \phi$, where $\phi \ll \mu$ is the adjusting value. Therefore, after n turns, approximately, the vector W only changes by a phase factor of $e^{in(\mu+\phi)}$,

$$W = e^{n(i\mu I + \tau)} W_0 \cong e^{in(\mu+\phi)} W_0. \quad (7)$$

From Eq. 7, we have

$$\tau W_0 \cong i\phi W_0. \quad (8)$$

Using the property of the Jordan matrix in Eq. 3, the above equation can be explicitly written as

$$\tau \begin{bmatrix} w_0 \\ w_1 \\ \dots \\ w_{m-1} \end{bmatrix} = \begin{bmatrix} w_1 \\ w_2 \\ \dots \\ 0 \end{bmatrix} \cong \begin{bmatrix} i\phi w_0 \\ i\phi w_1 \\ \dots \\ i\phi w_{m-1} \end{bmatrix}, \quad (9)$$

where w_j represents the j th row of W_0 . $i\phi$ is then derived by comparing the two sides,

$$i\phi = \frac{w_1}{w_0} \cong \frac{w_2}{w_1} \cong \frac{w_3}{w_2} \cong \dots \quad (10)$$

For a 6-D scenario, Eq. (7) is derived for the planes x , y , and z , resulting in three sets of polynomials w_{x0}, w_{x1}, \dots , w_{y0}, w_{y1}, \dots and w_{z0}, w_{z1}, \dots . These polynomials can be used as a set of approximated action-angle variables. Their trajectories form a circle with a small deviation from a rigid rotation. It was reported in [14] that near the boundary of the stable region, the deviation of these actions from a rigid rotation provides an important indicator of the destruction of invariant tori, which measures the stability of the trajectories.

B. Square matrix with eigen-decomposition

In realistic dynamical systems with strong nonlinearity and coupling terms, simply using Courant-Snyder variables in Eq. (1) does not necessarily result in an upper triangular square matrix M . To improve the precision of square matrix construction, we use a numerical decomposition of the transfer matrix M_x , the eigen-decomposition, to refactor M_x into a canonical form. The original transfer matrix is defined as

$$X = M_x X_0, \quad (11)$$

where X_0 represents the 6-D closed orbit of the lattice. With eigen-decomposition, M_x can be refactored as

$$M_x = V \Lambda V^{-1}, \quad (12)$$

where Λ is an upper triangular matrix.

Similarly, the new column Z can be written as $Z = V^{-1}X$. The square matrix in Section II.A is now replaced by Λ . Similar to Eq. (5), the W variable is defined as

$$W \equiv VZ. \quad (13)$$

Here W represents the same physical quantities as X , but expressed on the basis Z through the eigenvectors v_j , namely,

$$w_j = v_j Z. \quad (14)$$

C. Transformation from 6-D dynamical equation to action-angle variables

In the previous section, a transformation V is generated by eigen-decomposition to create a set of new variables w , so that the transfer map $\Lambda = V^{-1}M_xV$ is approximately a rigid rotation and w is approximated action-angle variables. Considering that the new set of w variables is not unique, for a 6-D dynamical system, we use v_1 , v_2 and v_3 to denote the approximated action-angle variables chosen. The simplest choice is $v_1 = w_{x0}$, $v_2 = w_{y0}$, and $v_3 = w_{z0}$, which can be rewritten as

$$v_j(\theta_j) \equiv e^{i\theta_j}, j = 1, 2, 3$$

where θ_1 , θ_2 and θ_3 are complex numbers denoting oscillations deviating from rigid rotations with frequencies ω_1 , ω_2 and ω_3 . The phase deviation is the real part of θ and the amplitude deviation is the imaginary part of θ .

Note that, unlike the standard definition in a Hamiltonian system, these approximated action-angle variables are a loose term, with their absolute values as actions and their phases as angles. This can be further loosely extended to use $\text{Re}(\theta)$ as angle and $\text{Im}(\theta)$. In the following discussion, the term "action-angle variables" refers only to the new variables θ_1 , θ_2 , θ_3 and their conjugates. The one-turn map of θ can be written as

$$\theta_{j,k+1} = \theta_{j,k} - i \log \frac{v_j(\theta_{j,k+1})}{v_j(\theta_{j,k})} \equiv \theta_{j,k} + \phi_j(\theta_{1,k}, \theta_{2,k}, \theta_{3,k}), j = 1, 2, 3 \quad (15)$$

When there are quasi-periodic solutions, the action-angle variables $(\theta_1, \theta_2, \theta_3)$ can be transformed to a rigid rotation $(\alpha_1, \alpha_2, \alpha_3)$ that satisfies

$$\alpha_{j,k+1} = \alpha_{j,k} + \omega_j, \quad j = 1, 2, 3, \quad (16)$$

where ω represents the rotation numbers of the rigid rotation. If we denote $\Delta\phi_i \equiv \phi_i - \omega_i$, $i = 1, 2, 3$, the equations of the action-angle variables $(\theta_1, \theta_2, \theta_3)$ become

$$\begin{aligned} \theta_j(\alpha_1 + \omega_1, \alpha_2 + \omega_2, \alpha_3 + \omega_3) - \theta_j(\alpha_1, \alpha_2, \alpha_3) = \\ \omega_j + \Delta\phi_j[\theta_1(\alpha_1, \alpha_2, \alpha_3), \theta_2(\alpha_1, \alpha_2, \alpha_3), \theta_3(\alpha_1, \alpha_2, \alpha_3)], \quad j = 1, 2, 3. \end{aligned} \quad (17)$$

To solve the exact equations, we use the zero-order approximation $\theta_i^{(0)} = \alpha_i$,

$$\begin{aligned} \theta_j^{(1)}(\alpha_1 + \omega_1, \alpha_2 + \omega_2, \alpha_3 + \omega_3) - \theta_j^{(1)}(\alpha_1, \alpha_2, \alpha_3) \approx \\ \omega_j^{(0)} + \Delta\phi_j[\theta_1^{(0)}(\alpha_1, \alpha_2, \alpha_3), \theta_2^{(0)}(\alpha_1, \alpha_2, \alpha_3), \theta_3^{(0)}(\alpha_1, \alpha_2, \alpha_3)] = \\ \omega_j^{(0)} + \Delta\phi_j(\alpha_1, \alpha_2, \alpha_3), \quad j = 1, 2, 3, \end{aligned} \quad (18)$$

where ω_j is the constant term of the Fourier transform of $\phi_j(\alpha_1, \alpha_2, \alpha_3)$.

In the vicinity of a pure rotation, KAM theory proved the existence of a pure rotation. In a practical solution, we can use the Truncated Power Series Algebra (TPSA) to calculate the transfer map and numerically iterate the perturbative equations above to monitor the difference between iterations. A convergent series solution can be used as an indicator to the existence of the quasi-periodic solution. If the convergence map blows up, it suggests that the trajectory has a large amplitude or is close to a resonance line.

III. APPLICATION ON A 6-D TOY MAP

Crab cavities are specialized RF cavities designed to retrieve head-on collisions in colliders for high luminosities. Here, we investigate a 6-D periodic system that includes a crab cavity

kick. A time-dependent sextupole kick is also incorporated into the crab cavity model as the multipole components in the cavity. The transfer map associated with the crab cavity can be expressed as

$$\delta p_x = -\frac{\tan(\theta_{cc}) \sin(k_c z)}{k_c \sqrt{\beta_{cc} \beta_{IP}}} + b_3(x^2 - y^2) \sin(k_c z) \quad (19)$$

$$\delta p_y = -2b_3 x y \sin(k_c z) \quad (20)$$

$$\delta p_z = -\frac{x \tan(\theta_{cc}) \cos(k_c z)}{\sqrt{\beta_{cc} \beta_{IP}}} + \frac{b_3 k_c}{3} (x^3 - 3xy^2) \cos(k_c z), \quad (21)$$

where θ_{cc} is the crossing angle, k_c is the wave number, b_3 is the strength of the time-dependent sextupole kick in the crab cavity, and β_{cc} and β_{IP} are beta functions at the crab cavity and the interaction point (IP), respectively. The rest of the periodic map is made up of pure rotations with tunes of $[\nu_x, \nu_y, \nu_z] = [0.26, 0.23, 0.005]$. These tune values satisfy the high-order resonance condition $2\nu_x + 2\nu_y + 4\nu_z = 1$, indicating potential resonance behaviors in the system.

To investigate the 6-D beam dynamics of the system, especially the synchro-betatron couplings, we generate a uniform grid of 100×100 particles in the x - z plane. The initial coordinates y of all particles are fixed at 0.5 mm, while the initial momenta p_x , p_y , and p_z are zero. The high-order transfer map for each particle is computed using JuTrack [23], a novel auto-differentiable simulation code developed in the Julia programming language. The resulting dynamics are then analyzed using the CM up to the third order. For comparison, the FMA method is also applied to this toy system. Particle trajectories are tracked for 50,000 turns, and the tune diffusion between the last 2,000 turns is used to calculate the frequency map.

Figure 1 presents the results of applying the CM method to the toy model and its comparison with the FMA method. The results show that CM successfully detects all resonances identified by FMA, validating its accuracy and effectiveness in characterizing 6-D nonlinear dynamics for this system. In particular, the CM method also reveals additional resonance structures not detected by FMA, such as the selected points highlighted in Fig. 1. These structures are located in regions where FMA indicates small tune diffusion, suggesting that FMA may miss certain subtle or high-order resonances.

Further insight is provided by the tune footprint shown in Fig. 2, where the highlighted points are found to cross the eighth-order resonance line $2\nu_x + 2\nu_y + 4\nu_z = 1$. This resonance

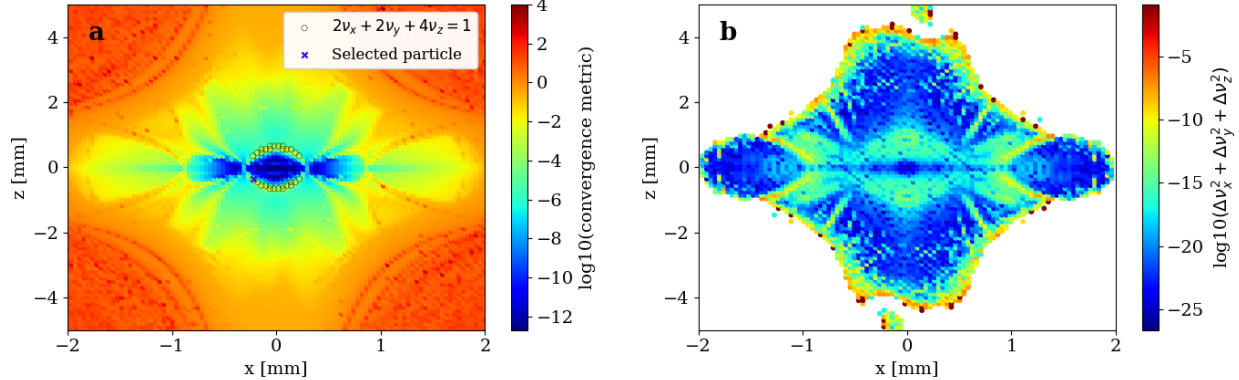


FIG. 1. CM and FMA results for the toy system in the x - z plane. The left plot shows the minimum difference between two successive iterations of the CM method. A large value of the convergence metric indicates divergence of the convergence map. The color scale in the right plot represents tune diffusion of the trajectories.

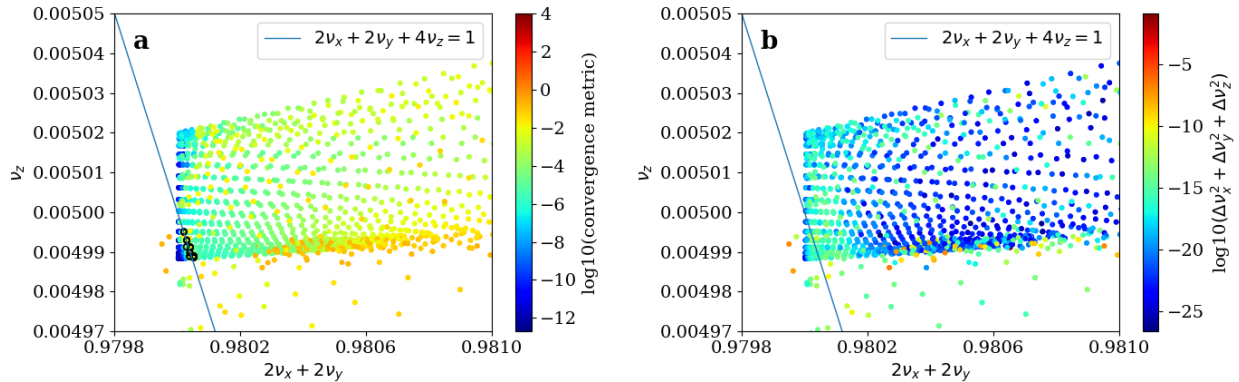


FIG. 2. Results of CM (left) and FMA (right) in the frequency space. The black circles in the left plot correspond to the black circles in spatial space shown in Fig. 1(a). The x-axis represents $2\nu_x + 2\nu_y$ and the y-axis represents ν_z .

is intentionally introduced into the model to test both methods. The CM method successfully identifies this eighth-order resonance, while the frequency map in this region remains relatively smooth. This result suggests a high sensitivity of the CM method to resonances, especially for high-order or subtle resonances.

IV. APPLICATION ON THE ELECTRON-ION COLLIDER

The design of the Electron-Ion Collider (EIC) aims to enable collisions between polarized electrons and a wide range of ion species, including spin-polarized protons at energies up to 275 GeV. The Hadron Storage Ring (HSR) of the EIC is designed to reuse much of the existing infrastructure from the Relativistic Heavy Ion Collider (RHIC) [24], with modifications to accommodate the requirements of the EIC physics program. In particular, crab cavities are employed in the EIC to restore head-on collisions for higher luminosity.

Evaluating the dynamic aperture (DA) of the HSR requires long-term particle tracking, typically over 10^6 turns, making it computationally expensive. To efficiently evaluate the DA and study the nonlinear beam dynamics of the HSR, the CM method is applied to the HSR lattice to analyze local stability across different slices in the phase space. The HSR lattice is constructed using JuTrack. Two pairs of crab cavities are included in the lattice model. For simplicity, we consider only a single pair of 197 MHz cavities in this study. Following the study of multipole components in the EIC crab cavities [25, 26], similar to Eq. (19-21), time-dependent sextupole components with geometric strength of 10^{-3} m^{-3} are added to the crab cavities.

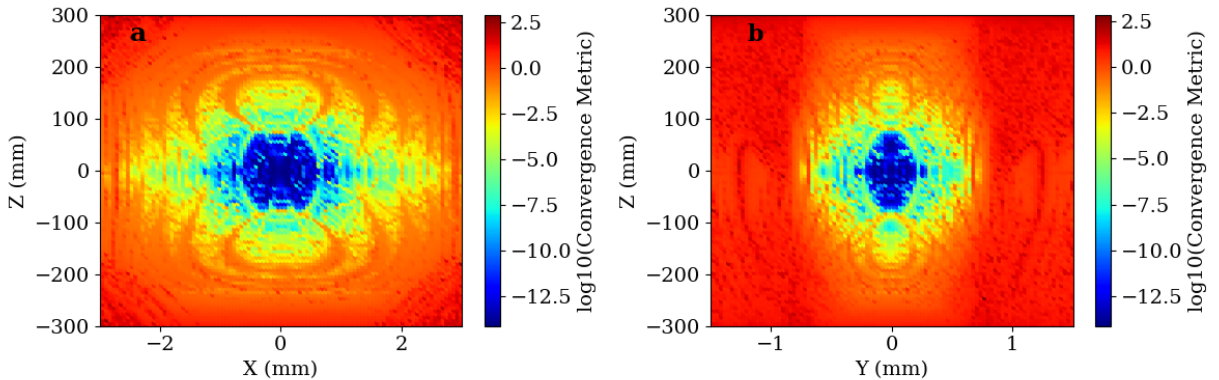


FIG. 3. CM analysis results for the EIC HSR in the x - z (left) and y - z (right) plane. The color scale from blue to red represents the convergence error to a rigid rotation increasing from small to large.

The CMs are calculated across different slices in the phase space. Specifically, we consider three slices in the x - y , x - z , and y - z planes, fixing the third coordinate at an RMS beam size (σ_z , σ_y , and σ_x , respectively). The scanning ranges are $[-3, 3]$ mm for x , $[-1.5, 1.5]$ mm for

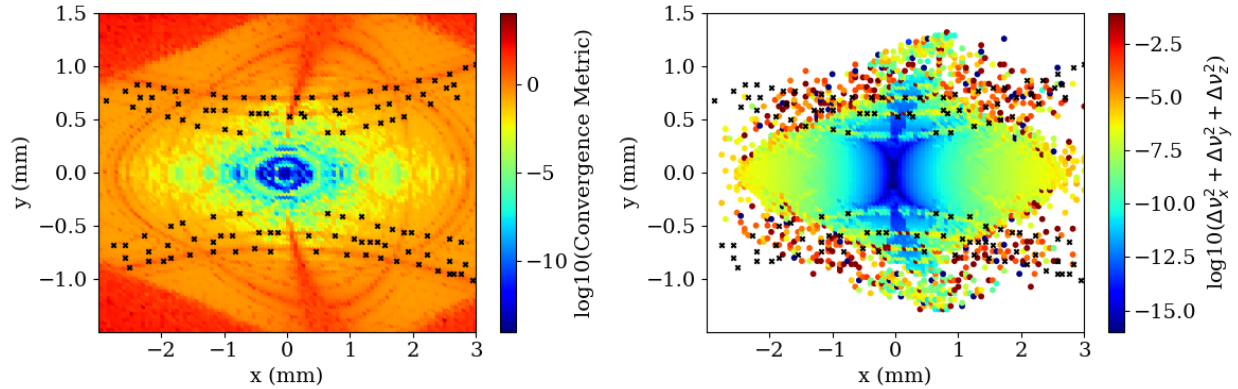


FIG. 4. Results of applying CM (left) and FMA (right) to the EIC HSR in the x - y plane. The initial z for all particles are fixed at 6 cm. The black points represent some selected trajectories crossing resonance lines.

y , and $[-30, 30]$ cm for z , covering a wide region in the space compared to the DA size. The initial momenta p_x , p_y and p_z are set to 0.

Figure 3 shows the CM evaluated in two longitudinal-transverse slices of the HSR phase space, x - z , and y - z . Dark blue regions correspond to strongly convergent solutions, indicating the existence of invariant tori and regular quasi-periodic motion, whereas yellow-red regions represent loss of convergence and are associated with resonance crossing or very large amplitude. Many orange/red patterns are observed in the plots that represent trajectories crossing some synchro-betatron resonance lines.

The CM analysis in the x - y plane (left panel of Fig. 4(a)) also exhibits distinct patterns. The red patterns in Fig. 4(a) illustrate the stable boundary that agree well with the boundary of the DA in the x - y space. Some trajectories having large residual convergence errors relative to a rigid rotation are highlighted in Fig. 4, and their locations are found to agree well with the resonance structures observed in the FMA results in Fig. 4(b). Using only the one-turn transfer map, the CM method therefore effectively probes the stable region, demonstrating both its efficiency and accuracy for DA evaluation.

Figure 5 shows the trajectories highlighted in Fig. 4 in frequency space. It is found that these selected points lie on three different resonance lines, including the linear transverse resonance $\nu_x = \nu_y$, and synchro-betatron resonances such as $\nu_x = \nu_y + \nu_z$ and $2\nu_x - 2\nu_y - \nu_z = 0$. These resonances strongly affect long-term beam stability and can lead to particle loss, indicating highly nonlinear dynamics in the ring.

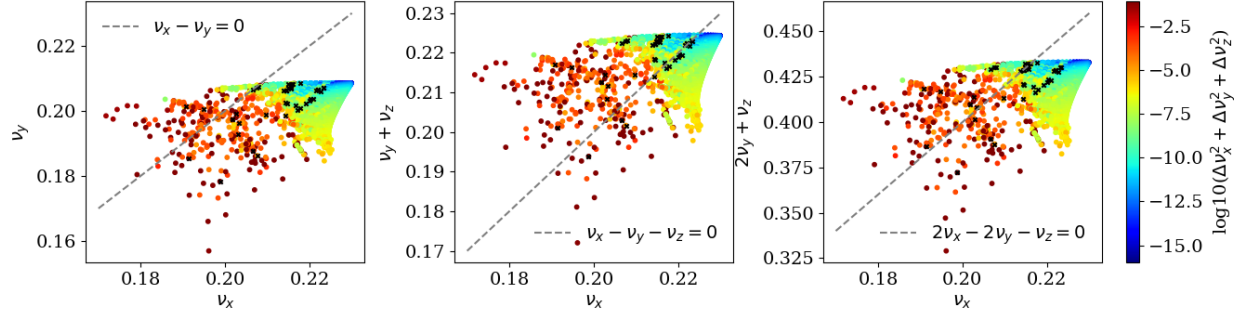


FIG. 5. FMA results in frequency space. The left plot shows the result in ν_x and ν_y space, the middle one shows the ν_x and $\nu_y + \nu_z$ space, and the right one shows the ν_x and $2\nu_y + \nu_z$ space. The black cross in the plots correspond to the selected points in Fig. 4.

To further study the impact of multipole components in crab cavities, we increase the sextupole strength from 10^{-3} m^{-3} to 10^{-2} m^{-3} . With the increased multipole components, both CM and FMA show a significant reduction in the DA size by nearly a factor of two in Fig. 6. This observation is consistent with previous findings [26, 27], revealing the sensitivity of beam dynamics to nonlinearities introduced by multipole components in crab cavities. Since the multipole components of the crab cavities are time dependent, traditional magnets cannot compensate for their nonlinear effects. Therefore, it is important to control the multipole strength during crab cavity design or use external magnets to cancel these effects to maintain sufficient DA.

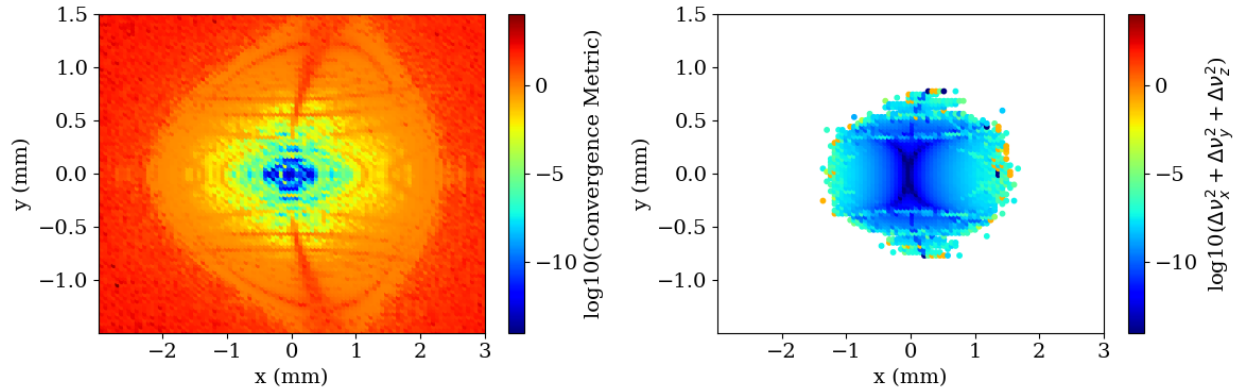


FIG. 6. Results of applying the CM method (left) and FMA (right) to the HSR with increased multipole components in the crab cavities. The strength of sextupole components in the crab cavity is increased to 10^{-2} m^{-3} .

V. CONCLUSION

The square matrix-based CM is extended to the full 6-D phase space to study nonlinear beam dynamics in ring accelerators. By reformulating the one-turn map to a square matrix representation through eigen-decomposition, a set of approximated action-angle variables are constructed. The residual convergence error from transforming the map into a rigid rotation is used as an indicator of trajectory stability.

We demonstrate that in a toy model with crabbing kicks, the 6-D CM successfully captures both known and undetected high-order resonances that are missed by the FMA. This method is then applied to the the EIC HSR, where it effectively identifies resonance structures that critically impact long-term beam stability. By increasing the strength of the multipole component in the crab cavities, a significant reduction in DA is observed. The CM exhibits excellent agreement with the FMA results in evaluating the resonance structures of the HSR. Compared to particle tracking simulation that can require more than 10^6 turns of tracking, the CM method allows efficient evaluation of long-term beam stability with the one-turn transfer map, significantly reducing the evaluation time of the DA.

This work establishes the 6-D CM method as a fast and accurate tool for nonlinear beam dynamics analysis. Its ability to detect high-order resonances and efficient evaluation of DA boundaries from one-turn map makes it a promising approach for future accelerator design, optimization, and long-term stability studies.

ACKNOWLEDGMENTS

This work is supported by the DOE Office of Science, with award number DE-SC0024170.

- [1] A. J. Lichtenberg and M. A. Lieberman, *Regular and chaotic dynamics*, Vol. 38 (Springer Science & Business Media, 2013).
- [2] R. D. Ruth, *Single particle dynamics in circular accelerators*, Tech. Rep. (Stanford Linear Accelerator Center, Menlo Park, CA (USA), 1986).
- [3] G. Guignard, *A general treatment of resonances in accelerators*, Tech. Rep. (European Organization for Nuclear Research, 1978).

- [4] A. Schoch, *Theory of linear and non-linear perturbations of betatron oscillations in alternating-gradient synchrotrons*, Tech. Rep. (Cern, 1958).
- [5] A. J. Dragt, Lie algebraic methods for charged particle optics, in *AIP Conference Proceedings*, Vol. 177 (American Institute of Physics, 1988) pp. 261–264.
- [6] M. Berz, Differential algebra-a new tool, in *Proceedings of the 1989 IEEE Particle Accelerator Conference, Accelerator Science and Technology* (IEEE, 1989) pp. 1419–1423.
- [7] A. W. Chao, *Lecture notes on topics in accelerator physics*, Tech. Rep. (SLAC National Accelerator Lab., Menlo Park, CA (United States), 2002).
- [8] A. Bazzani, G. Servizi, G. Turchetti, and E. Todesco, *A normal form approach to the theory of nonlinear betatronic motion*, CERN-94-02 (CERN, 1994).
- [9] E. Forest, J. Irwin, and M. Berz, Normal form methods for complicated periodic systems: a complete solution using differential algebra and lie operators, *Part. Accel.* **24**, 91 (1989).
- [10] J. Laskar, Frequency map analysis and particle accelerators, in *Proceedings of the 2003 Particle Accelerator Conference*, Vol. 1 (IEEE, 2003) pp. 378–382.
- [11] Y. Li, J. Wan, A. Liu, Y. Jiao, and R. Rainer, Data-driven chaos indicator for nonlinear dynamics and applications on storage ring lattice design, *Nuclear Instruments and Methods in Physics Research Section A: Accelerators, Spectrometers, Detectors and Associated Equipment* **1024**, 166060 (2022).
- [12] J. Wan and Y. Jiao, Machine learning enabled fast evaluation of dynamic aperture for storage ring accelerators, *New Journal of Physics* **24**, 063030 (2022).
- [13] L. H. Yu, Analysis of nonlinear dynamics by square matrix method, *Physical Review Accelerators and Beams* **20**, 034001 (2017).
- [14] L. H. Yu, Y. Hidaka, V. Smaluk, K. Anderson, and Y. Hao, Convergence map with action-angle variables based on square matrix for nonlinear lattice optimization, *Physical Review Accelerators and Beams* **26**, 054002 (2023).
- [15] K. Anderson, Y. Hao, L. H. Yu, *et al.*, Study of nonlinear dynamics in the 4-d hénon map using the square matrix method and iterative methods, in *Proc. 5th North American Particle Accel. Conf. (NAPAC'22)* (2022) pp. 232–235.
- [16] L. H. Yu, Y. Li, and L. Yang, Theory of square matrix for nonlinear optimization, and application to nsls-ii, in *Nonlinear Dynamics and Collective Effects in Particle Beam Physics: Proceedings of the International Committee on Future Accelerators Arcidosso Italy 2017* (World

Scientific, 2019) pp. 12–22.

[17] L. Yu, Y. Hidaka, F. Plassard, V. Smaluk, and Y. Hao, Progress on convergence map based on square matrix for nonlinear lattice optimization, in *Proc. of the 5th North American Particle Accelerator Conf.(NAPAC'22), Albuquerque, NM* (2022).

[18] J. Berg, C. Liu, H. Lovelace III, S. Peggs, G. Robert-Demolaize, N. Tsoupas, and D. Xu, *Lattice design for the hadron storage ring of the Electron-Ion Collider*, Tech. Rep. (Brookhaven National Laboratory (BNL), Upton, NY (United States), 2023).

[19] A. Alekou, R. Appleby, E. Cruz-Alaniz, H. Bartosik, M. Carlà, S. Kostoglou, and Y. Papaphilippou, Long term stability studies in the presence of crab cavities and high order multipoles in the cern super proton synchrotron and high luminosity large hadron collider, *Nuclear Instruments and Methods in Physics Research Section A: Accelerators, Spectrometers, Detectors and Associated Equipment* **1050**, 168178 (2023).

[20] D. Xu, Y. Luo, C. Montag, Y. Hao, and J. Qiang, Study of harmonic crab cavity in eic beam-beam simulations, in *Proceedings of the 12th International Particle Accelerator Conference (IPAC'21), Campinas, Brazil* (2021).

[21] B. Kågström and A. Ruhe, An algorithm for numerical computation of the jordan normal form of a complex matrix, *ACM Transactions on Mathematical Software (TOMS)* **6**, 398 (1980).

[22] H. Broer, Kam theory: the legacy of kolmogorov's 1954 paper, *Bulletin of the American Mathematical Society* **41**, 507 (2004).

[23] J. Wan, H. Alamprese, C. Ratcliff, J. Qiang, and Y. Hao, Jutrack: A julia package for auto-differentiable accelerator modeling and particle tracking, *Computer Physics Communications* **309**, 109497 (2025).

[24] M. Harrison, S. Peggs, and T. Roser, The rhic accelerator, *Annual Review of Nuclear and Particle Science* **52**, 425 (2002).

[25] Q. Wu, S. De Silva, Y. Luo, J. Mitchell, B. Xiao, *et al.*, Eic crab cavity multipole analysis, in *12th International Particle Accelerator Conference (IPAC'21), Campinas, SP, Brazil* (JACOW Publishing, Geneva, Switzerland, 2021) pp. 2589–2591.

[26] Q. Wu, Y. Luo, B. Xiao, S. De Silva, and Z. Li, Eic crab cavity multipole analysis and their effects on dynamic aperture, in *13th International Particle Accelerator Conference (IPAC'22), Bangkok, Thailand* (2022) pp. 66–69.

[27] J. Barranco García, R. De Maria, A. Grudiev, R. Tomás García, R. Appleby, and D. Brett,

Long term dynamics of the high luminosity large hadron collider with crab cavities, Physical Review Accelerators and Beams **19**, 101003 (2016).